Minireviews
doi.org/10.1002/batt.201900230

Chemistry Europe
European Chemical Societies Publishing

Symmetric, Asymmetric, and Battery-Type Supercapacitors Using Two-Dimensional Nanomaterials and Composites

Jayesh Cherusseri,[a] Deepak Pandey,[a, b] and Jayan Thomas*[a, b, c]

Recent advances in the field of energy storage devices such as supercapacitors and batteries have helped mankind to cater to their power demands to a greater extent. 2D materials-based electrodes have attracted great interest in the recent past due to their unique properties such as large surface area, good electronic conductivity, excellent electrochemical properties, and good chemical, electrochemical, and thermal stabilities, which are essential requirements for a supercapacitor electrode to obtain high-performance. In this review, we discuss the recent advancements in the field of 2D materials such as MXenes, transition metal dichalcogenides, phosphorene, and their composites as electrodes in high-performance supercapacitors. The electrochemical performances of these 2D materials-based electrodes in symmetric, asymmetric, and battery-type hybrid supercapacitors are reviewed. Emphasis is given to the recent developments on the battery-type hybrid supercapacitors fabricated using these 2D materials-based electrodes. The future perspectives of these materials in the next-generation energy storage are also briefly discussed.

1. Introduction

The social, environmental and economic problems affiliated with the usage of fossil fuels can be solved by using alternative renewable power systems such as solar, wind, tidal, thermal, etc.[1] Around the globe, people have witnessed the soaring need of cheap and reliable energy for daily use. Renewable energy conversion technologies face a major challenge of discontinuous energy production, which has led to a disrupted supply of energy.[2] The output electrical energy from these sources is intermittent and not delivered continuously to both domestic and industrial applications. Hence contemporary electrical energy storage systems have acquired much importance to resolve the requirement of continuous energy production-distribution barriers. Classical energy storage devices such as lead-acid and metal-ion (lithium-ion, sodium-ion, etc.) batteries have limitations like low power densities and inferior cycle life, although they exhibit high energy densities. To eradicate this, electrochemical capacitors or supercapacitors (otherwise known as ultracapacitors) have been evolved.[3] High-power supercapacitors have been developed in the recent past to fulfill the needs of a variety of devices ranging from a tiny on-chip energy storage devices[4] to hybrid-electric vehicles.[5]

Unlike the conventional capacitors, the supercapacitors store charges electrochemically but exhibits high energy density compared to the former. Supercapacitors utilize large surface area electrodes to achieve maximum electrochemical performances and a variety of electrolytes to achieve a cell voltage.[6] A supercapacitor with water-based electrolytes can operate at a maximum voltage of 1.23 V, whereas using the organic or ionic liquids provide more than 3 V.[7] In advanced energy storage systems, a combination of supercapacitor and battery are envisaged to obtain both high power and energy densities.[8] Based on the charge storage mechanisms, supercapacitors are divided into two categories, namely, electrochemical double-layer capacitors (EDLCs) and pseudocapacitors.[9] In EDLCs, the charges are stored at the electrode/electrolyte interface by forming electrochemical double layers. In pseudocapacitors, the supercapacitor electrodes undergo fast redox reactions with the electrolyte-ions.[10] Advancements in the nanoscience and nanotechnology lead to considerable improvement in the electrochemical performances of the supercapacitors. This is due to the enhanced surface area of the electrodes to store charges and easy diffusion of the electrolyte into the nanostructured electrodes. Carbon nanomaterials such as graphene and carbon nanotubes are typical examples of the electrodes used in EDLCs.[11] Transition metal oxides and hydroxides, electronically conducting polymers, MXenes, transition metal dichalcogenides (TMDs), metal-organic frameworks are examples of a few pseudocapacitor electrode materials. Among the various electrode nanostructures, two-dimensional (2D) materials have received immense interest in using them as supercapacitor electrode material due to various reasons. A major factor is their large surface area associated with the 2D materials and it is well studied that the specific capacitance of a supercapacitor is directly related to the effective surface area of the electrodes. When compared with zero dimensional and one-dimensional nanostructures, 2D nanostructures possess large surface area

[a] Dr. J. Cherusseri, D. Pandey, Prof. J. Thomas
Nanoscience Technology Center
University of Central Florida, Orlando, FL-32826, USA
[b] D. Pandey, Prof. J. Thomas
Materials Science and Engineering
University of Central Florida, Orlando, FL-32816, USA
[c] Prof. J. Thomas
College of Optics and Photonics
University of Central Florida, Orlando, FL-32816, USA
E-mail: Jayan.Thomas@ucf.edu

This publication is part of a joint Special Issue with ChemSusChem focusing on "2D Energy Storage Materials"

and typical examples are MXenes, TMDs, and a recently explored material, phosphorene.

Based on the electrode configurations in a supercapacitor, they are classified as symmetric, asymmetric and battery-type supercapacitors. A symmetric supercapacitor utilizes two similar electrodes, whereas an asymmetric supercapacitor uses two different materials for electrodes. The third type, known as a battery-type hybrid supercapacitor, uses a battery electrode and a supercapacitor electrode also attracted considerable scientific interest due to their superior energy densities. The high energy density is obtained since metal-ions (such as lithium-ion and sodium-ion) are intercalated within the electrode nanostructure for the charge storage.[12] Battery-type hybrid supercapacitors are potential candidates for long-lasting power supplies compared with the conventional supercapacitor electrodes, but a major hurdle lies in the charge balancing of the two electrodes. They can bridge the gap between supercapacitors and batteries. This minireview focuses on the recent developments of the 2D materials such as MXenes, TMDs, and phosphorene-based electrodes in symmetric, asymmetric, and battery-type hybrid supercapacitors. Novel battery-type hybrid supercapacitor configurations based on these 2D material electrodes and their electrochemical performances are also included. A schematic diagram showing the outline of the present review is represented in Figure 1.

2. Two-Dimensional MXenes in Supercapacitors

MXenes, a class of 2D materials consisting of transition metal carbides, emerged as layered materials with unique properties such as large surface area, good in-plane electronic conductivity, chemically-active hydrophilic edges.[13] From the early time of its inception, they have attracted scientific interest in supercapacitor communities and explored them as electrode materials for both lithium-ion batteries and supercapacitors.[14] MXenes offer good electrical conductivity, which is a major advantage of using these materials. But the main disadvantage of using this 2D MXene is the self-restacking of individual nanosheets resulting in a graphite-like structure. Hence the pristine 2D MXene nanosheets are not preferred for high-performance supercapacitor electrode applications. Pristine 2D Ti_2CT_x MXene nanosheets were used as electrodes for supercapacitor applications in the recent past.[15] Due to the self-restacking issue associated with the 2D Ti_2CT_x MXene nanosheets, a low capacitance of 51 F/g was obtained for the symmetric supercapacitor at a current density of 1 A/g. But this supercapacitor exhibited a maximum rate performance of 86% and good cycling stability of 6000 cycles with capacitance retention of 93%.

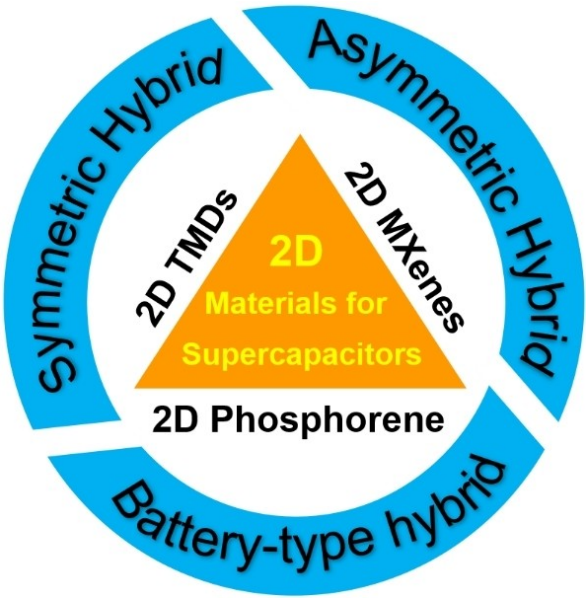

Figure 1. Schematic diagram showing various 2D material-based electrodes in symmetric, asymmetric, and battery-type hybrid supercapacitors.

2.1. 2D MXene Electrodes for Symmetric Supercapacitors

To avoid the self-restacking of pristine 2D MXenes, hybrid electrode structures are usually fabricated using different materials such as transition metal-oxides and electronically conducting polymers. The as-fabricated hybrid electrodes exhibit superior properties when compared with their individual material counter-parts. 2D Ti_3C_2 MXene synthesized by the wet-chemical route was used to prepare free-standing MnO_x–Ti_3C_2 hybrid films with high flexibility for supercapacitor applications.[16] The incorporation of MnO_x is found to prevent the self-restacking of the delaminated Ti_3C_2 nanosheets. A symmetric supercapacitor was fabricated using two identical free-standing MnO_x–Ti_3C_2 hybrid films and 1 M Li_2SO_4 solution to get a cell voltage of 1 V. The near-rectangular CV curves at different scan rates (Figure 2a) of the supercapacitor display good charge storage capability. The GCD curves at different current densities (Figure 2b) represent typical linear voltage-time profiles of a supercapacitor showing good electrochemical reversibility of the hybrid electrode. A low internal resistance was observed for the MnO_x–Ti_3C_2 supercapacitor electrode (Figure 2c). The symmetric supercapacitor exhibited an excellent specific energy density of 13.64 mWh/cm^3 at 2 mV/s. A high power density of 3755.61 mW/cm^3 was also obtained when tested at a scan rate of 100 mV/s. The supercapacitor displayed a good cycling stability of 10000 cycles with capacitance retention of 89.8%. The Ragone plot of the supercapacitor shown in Figure 2d and the cycling performance is shown in Figure 2e. The GCD curves (inset of Figure 2e) and CV curves (Figure 2f) before and after cycling represent no change in their profiles while maintaining the integrity of the electrode nanostructure (inset of Figure 2f) which illustrates its potential in the next-generation supercapacitors.

Nanocrystalline ε-MnO_2 nanowhiskers were deposited on two different 2D titanium carbide nanosheets, Ti_2CT_x and $Ti_3C_2T_x$ to prepare hybrid electrodes for symmetric supercapacitors.[17] The inclusion of ε-MnO_2 nanowhiskers is found to enhance the electrochemical performance of the 2D MXene hybrid electrodes by providing fast electrolyte-ion pathways through the

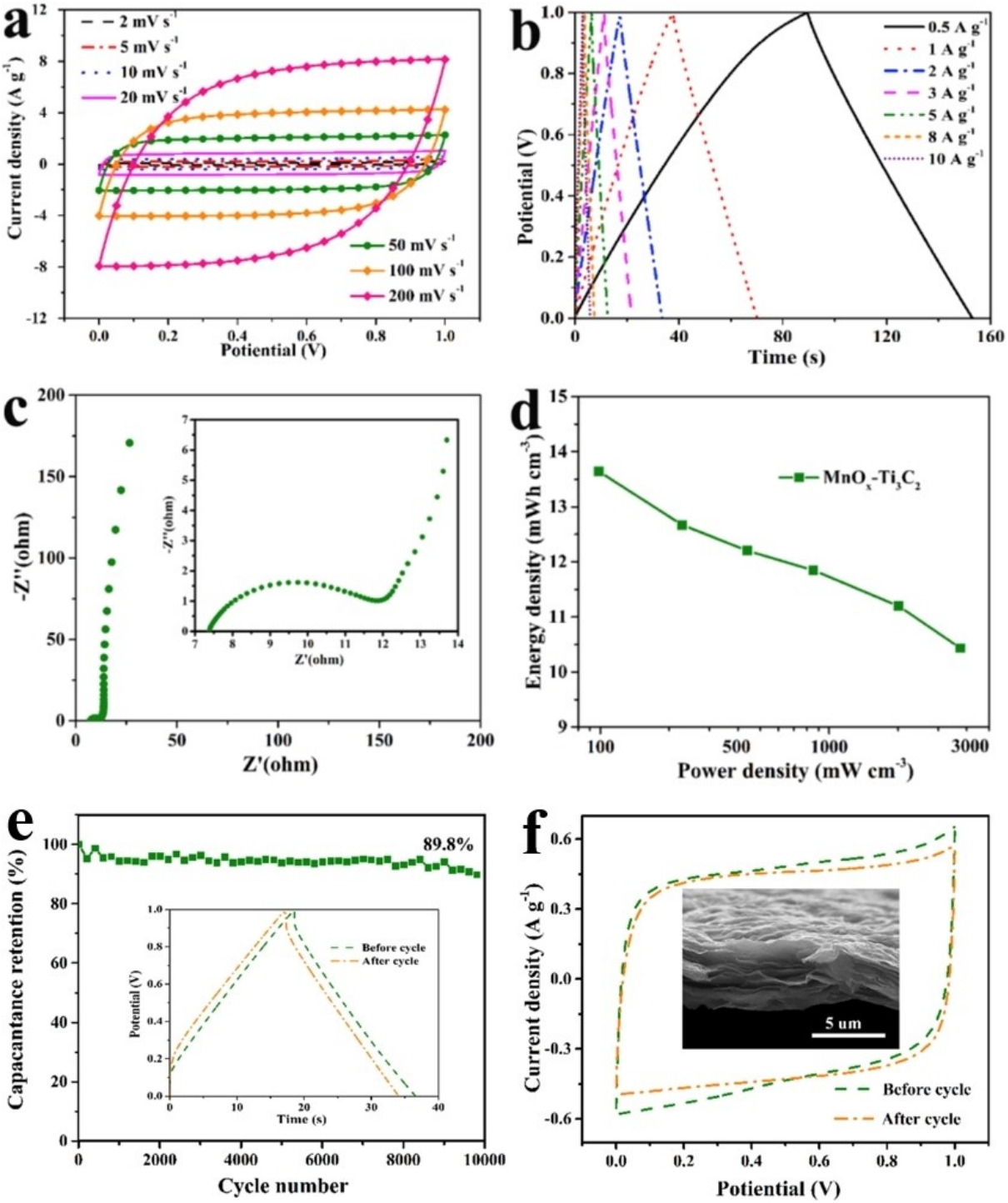

Figure 2. a) CV curves at different scan rates and b) GCD curves at different current densities of the MnO_x–Ti_3C_2 symmetric supercapacitor c) Nyquist plot (inset shows the magnified high-frequency region) of the MnO_x-Ti_3C_2 film electrode obtained in a three-electrode cell configuration within a frequency range of 10^5–10^{-3} Hz. d) Ragone plot of the MnO_x–Ti_3C_2 symmetric supercapacitor. e) Plot of capacitance retention vs. cycle number of the MnO_x–Ti_3C_2 symmetric supercapacitor, inset image shows the GCD curves obtained before and after cycling study. f) CV curves of the MnO_x–Ti_3C_2 symmetric supercapacitor before and after cycling, inset image shows the SEM image of the MnO_x–Ti_3C_2 film after cycling. Reproduced with permission from Ref. [16] Copyright (2017) Elsevier B.V.

nanosheets. The ε-MnO_2/Ti_2CT_x and ε-MnO_2/$Ti_3C_2T_x$ hybrid supercapacitors exhibited superior electrochemical performances when compared with pristine Ti_2CT_x and $Ti_3C_2T_x$ symmetric supercapacitors. The deposition of pseudocapacitive ε-MnO_2 on the surfaces of the 2D MXene nanosheets could enhance the charge storage ability by taking part in the faradaic reactions. A maximum specific capacitance of 212 F/g (Figure 3a) was achieved for the ε-MnO_2/$Ti_3C_2T_x$ hybrid super-

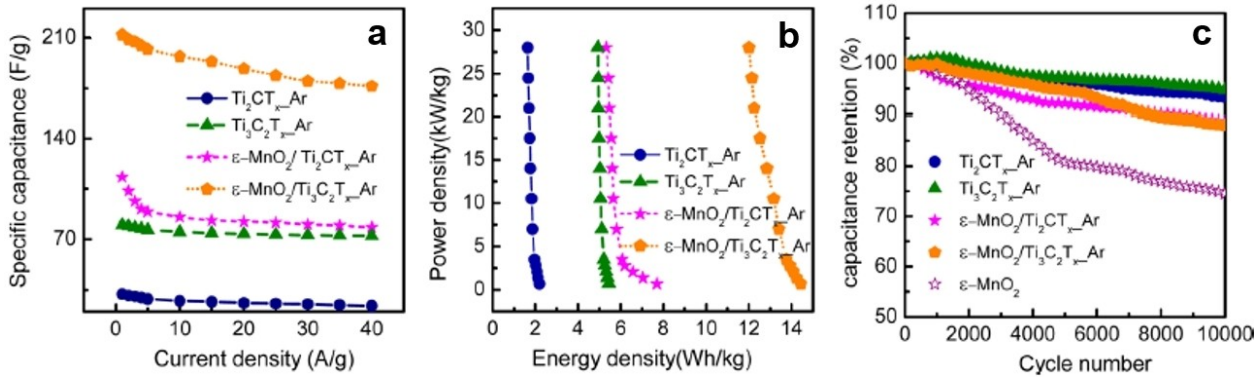

Figure 3. a) Plot of specific capacitance vs. current density, b) Ragone plot, and c) plot of capacitance retention vs. cycle number for the Ti_2CT_x and $Ti_3C_2T_x$, ε–MnO_2/Ti_2CT_x, and ε–MnO_2/$Ti_3C_2T_x$ supercapacitors. Reproduced with permission from Ref. [17] Copyright (2016) American Chemical Society.

capacitor at a current density of 1 A/g when tested in a CR2032 coin cell assembly using the aqueous electrolyte. Ragone plot (Figure 3b) demonstrates that the power density of the ε-MnO_2/$Ti_3C_2T_x$ hybrid supercapacitor is superior to the ε-MnO_2/Ti_2CT_x, Ti_2CT_x, and $Ti_3C_2T_x$ supercapacitors. The 2D MXene hybrid supercapacitors also exhibited excellent electrochemical cycling stability of 10000 cycles with capacitance retention of about 88%.

Polypyrrole (PPy) has been extensively used in flexible supercapacitors due to its high flexibility and electrochemical activity, but its low capacitance and poor cycling stability restrict its potential for applications in flexible supercapacitors.[18] Making a hybrid with MXenes can increase its capacitance and improve its cycling stability. In an attempt to improve cycling stability, a novel approach of creating a free-standing and conductive hybrid film by intercalating PPy into the layered structure of Ti_3C_2 (l–Ti_3C_2, an MXene material) was followed.[19] Upon the electrochemical characterization of the PPy/l–Ti_3C_2 electrode (FTO glass as the current collector), it was observed that specific areal capacitance was increased from 150 F cm^{-2} to 203 F cm^{-2} and the electrode was able to retain 100% of its capacitance for almost 20,000 cycles. Two of these free-standing PPy/l–Ti_3C_2 electrode films were used to fabricate an ultrathin all-solid-state symmetric supercapacitor using polyvinyl alcohol with sulfuric acid (PVA–H_2SO_4) gel electrolyte. This all-solid-state, symmetric flexible supercapacitor delivered an excellent areal capacitance of 35.6 mF cm^{-2} at a current density of 0.3 mA cm^{-2}. In the relaxed state, the device almost retained 100% of its capacitance for 10,000 charge-discharge cycles.

MXenes have also been used for fabricating micro-supercapacitors (MSC), which are very popular among wearable and flexible electronics. Recently, with the help of strain engineering and controlling the interlayer spacing, a free-standing MXene (fully laminated few-layered 2D $Ti_3C_2T_x$) based bacterial cellulose (BC) composite has been fabricated, which shows very high mechanical and electrochemical performance.[20] A simple all solution-based paper making process was used to fabricate the composite paper followed by a laser cutting kirigami process, which resulted in a unique stretchable interdigitated microstructure. A PVA-H_2SO_4 gel electrolyte was drop-casted onto this interdigitated structure to form an all-solid-state bendable, twistable, and stretchable MSC. This device exhibited an outstanding areal capacitance of 111.5 mF cm^{-2} at a current density of 2 mA cm^{-2} and was perfectly stable even during 100% elongation, bending, and twisting states. The charge-discharge cycling performance was relatively moderate, showing 72.2% retention after 5000 cycles. But this cycling was also accompanied by repeated deformation ranging from 0% to 100%, which could be a reason for a moderate to low cycling stability.

In another work, all MXene (2D Titanium Carbide) based solid-state MSC was fabricated using a solution spray coating of L–$Ti_3C_2T_x$ as the current collector layer directly on to glass surface and s–$Ti_3C_2T_x$ as the active material layer on top, followed by a photoresist free direct laser cutting to etch the interdigitated structure.[21] The bottom layer of L–$Ti_3C_2T_x$ had larger flakes (3–6 μm), therefor pre abbreviated by "L." These were used to serve as a current collector. The top layer of s–$Ti_3C_2T_x$ had smaller flake sizes, approximately. 1 μm ("s" stands for small) with a large number of defects and edges to serve as electroactive sites. PVA–H_2SO_4 gel was used as a solid polymer electrolyte. Compared to supercapacitors using $Ti_3C_2T_x$ and platinum as the current collector electrodes, all MXene devices showed lower contact resistance, higher specific capacitance and better rate capabilities. Attractive properties like high areal capacitance (27 mF/cm^{-2}) and volumetric capacitance (357 mF/cm^{-3}) were obtained at a scan rate of 20 mVs^{-1}. The device also retained 100% of its capacitance for almost 10,000 cycles at a scan rate of 50 mVs^{-1}.

Using a combination of technologies like laser printing, vacuum-assisted deposition, and physical sputtering, a $Ti_3C_2T_x$ MXene based all-solid-state flexible MSC was fabricated.[22] An A4 size printing paper was used as a substrate for laser patterning. Through the electrochemical characterization of the fabricated MSC, the device exhibited a maximum areal capacitance of 27.92 mF/cm^{-2} at a current density of 0.25 mA/cm^{-2}. The report claims that the value is 460% higher than an advanced carbon-based planar symmetric MSCs.

2.2. 2D MXene Electrodes for Asymmetric Supercapacitors

Asymmetric supercapacitor geometry consists of two different kinds of electrodes. Based on the electrochemical potential of the individual electrodes, the aqueous electrolyte decomposition potential window can be extended beyond 1.23 V. MXene electrodes are generally used as anode materials in constructing asymmetric supercapacitors and various other materials are used as cathode materials such as electronically conducting polymers, carbon nanomaterials, their composites, etc. Asymmetric supercapacitors were fabricated using all-pseudocapacitive organic-inorganic electrodes consisting of MXene cathodes and rGO-polymer anodes and they can operate at a cell voltage of 1.45 V in 3 M H_2SO_4 aqueous electrolyte.[23] Redox polymers such as polyaniline, polypyrrole and poly(3,4-ethylenedioxythiophene) were deposited on reduced graphene oxide (rGO) and further used as cathodes in assembling asymmetric supercapacitors. The PANI@rGO//$Ti_3C_2T_x$, polypyrrole@rGO//$Ti_3C_2T_x$, and PEDOT@rGO//$Ti_3C_2T_x$ asymmetric supercapacitors exhibited nearly symmetric GCD curves, as shown in Figure 4a-c with negligible voltage drop. Specific capacitances of 57, 59, and 47 F/g were obtained for PANI@rGO//$Ti_3C_2T_x$, polypyrrole@rGO//$Ti_3C_2T_x$, and PEDOT@rGO//$Ti_3C_2T_x$ asymmetric supercapacitors when tested at a scan rate of 5 mV/s. A Ragone plot of these supercapacitors is given in Figure 4d, which shows that PANI@rGO//$Ti_3C_2T_x$ asymmetric supercapacitor exhibited higher energy and power densities when compared to that of the other two devices. The PANI@rGO//$Ti_3C_2T_x$ asymmetric supercapacitor exhibited superior electrochemical cycling stability when compared to the other two devices. Capacitance retentions of 88.42, 75, and 80% were observed after 20000 cycles for the PANI@rGO//$Ti_3C_2T_x$, polypyrrole@rGO//$Ti_3C_2T_x$, and PEDOT@rGO//$Ti_3C_2T_x$ asymmetric devices, respectively.

All pseudocapacitive MXene-RuO_2 in-plane asymmetric MSC device with a cell voltage of 1.5 V was reported recently.[24] The asymmetric supercapacitor exhibited a specific capacitance of 93 F/g at a scan rate of 50 mV/s and was able to maintain a capacitance of 78 F/g when the scan rate is increased to 1000 mV/s in 1 M H_2SO_4 aqueous electrolyte. CV profiles obtained at different scan rates (Figure 5a) such as 5, 10, and 20 mV/s possessed large areas under the curves, which shows good charge storage capabilities. Ragone plot (Figure 5b) shows that the MXene-RuO_2 asymmetric supercapacitor device possesses superior energy and power densities when compared to in-plane pseudocapacitive asymmetric MSC in the literature. This asymmetric device could deliver an energy density of 19 μWh/cm^2 at a power density of 1.5 mW/cm^2. The tandem in-plane devices fabricated with two MXene-RuO_2 in-plane asymmetric devices connected in series exhibited CV profiles with a large area (Figure 5c) which shows an enhanced charge storage ability with an operating voltage of 3 V. Recently, an all-solid-state asymmetric supercapacitor was fabricated with Co_3O_4-MXene/rGO (3:1 ratio) hybrid porous aerogels (CMR31) as positive electrode and activated carbon (AC)-coated nickel foam as negative electrode.[25] The CMR31//AC asymmetric supercapacitor device could operate at a voltage of 1.6 V in 6 M KOH aqueous electrolyte and obtained a high energy density of 8.25 Wh/kg at a corresponding power density of 159.94 W/kg.

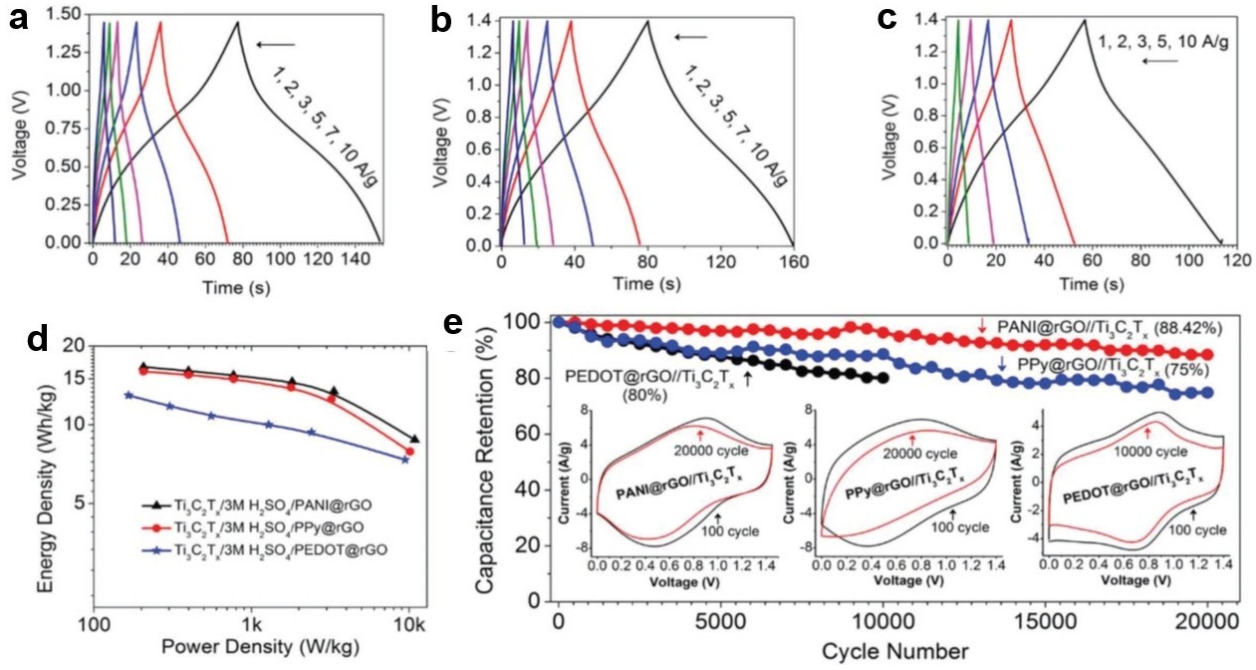

Figure 4. GCD curves of asymmetric supercapacitors: a) PANI@rGO//$Ti_3C_2T_x$, b) polypyrrole@rGO//$Ti_3C_2T_x$, and c) PEDOT@rGO//$Ti_3C_2T_x$. d) Ragone plot of PANI@rGO//$Ti_3C_2T_x$, polypyrrole@rGO//$Ti_3C_2T_x$, and PEDOT@rGO//$Ti_3C_2T_x$ asymmetric supercapacitors. e) A plot of capacitance retention at different cycle numbers of PANI@rGO//$Ti_3C_2T_x$, polypyrrole@rGO//$Ti_3C_2T_x$, and PEDOT@rGO//$Ti_3C_2T_x$ asymmetric supercapacitors (inset images represent the corresponding CV curves before and after the electrochemical cycling of the asymmetric supercapacitors). Reproduced with permission from Ref. [23]. Copyright (2018) WILEY-VCH Verlag GmbH & Co. KGaA, Weinheim.

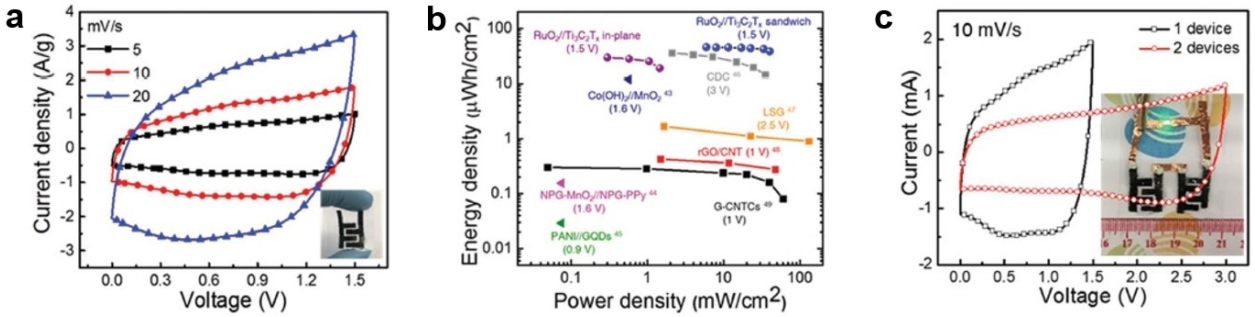

Figure 5. RuO_2//$Ti_3C_2T_x$ full-cell device: a) CV curves at different scan rates such as 5, 10, and 20 mV/s, b) Ragone plot and c) CV curves of single device and two devices connected in series (inset images show the digital photographs of the two asymmetric supercapacitor devices connected in series lighting-up a light-emitting diode). Reproduced with permission from Ref. [24]. Copyright (2018) WILEY-VCH Verlag GmbH & Co. KGaA, Weinheim.

Biscrolled MXene/carbon nanotube (BMX) yarn asymmetric supercapacitors with high-performance was reported recently.[26] The asymmetric supercapacitor was fabricated using the BMX yarn as anode and a biscrolled RuO_2/carbon nanotube yarn as the cathode. This asymmetric supercapacitor was able to achieve a cell voltage of 1.5 V when 3 M H_2SO_4 aqueous electrolyte was used. The specific capacitances of 203 F/cm^3, 554 mF/cm^2, 123 F/g, and 27.8 mF/cm were obtained at a current density of 2 mA/cm^2. No significant change in the capacitance was observed after performing electrochemical cycling for 10,000 cycles, which shows its resilience in real applications. A maximum power density of 5428 mW/cm^3 was obtained for the asymmetric device with a corresponding energy density of 11.9 mWh/cm^3.

A 3D porous MXene/bacterial cellulose (BC) self-supporting film was used as an anode to fabricate an asymmetric supercapacitor with polyaniline/BC as the cathode in 3 M H_2SO_4 aqueous electrolyte.[27] This aqueous asymmetric supercapacitor exhibited an areal capacitance of 925 mF/cm^2 with an energy density of 2.12 mW/cm^2 and a corresponding power density of 151 μWh/cm^2). The as-fabricated asymmetric device was flexible and was able to bend at an angle of 180° without any change in its electrochemical performances. An all-solid-state asymmetric supercapacitor device was also fabricated with the same set of electrodes (cathode and anode) and polyvinyl alcohol/H_2SO_4 gel electrolyte, which could deliver an areal capacitance of 585 mF/cm^2 and a gravimetric capacitance of 55 F/g. An all-solid-state asymmetric MSC was fabricated with coal-derived porous carbon as the negative electrode, MXene as the positive electrode, and polyvinyl alcohol/LiCl as solid-state polymer electrolyte.[28] This carbon/MXene asymmetric MSC device was able to operate in a voltage window of 0–0.8 V and exhibited good charge-storage capabilities. In a similar manner, an all-solid-state zinc/MXene hybrid asymmetric MSC was assembled using polyvinyl alcohol/Zn$(CF_3SO_3)_2$ polymer gel electrolyte.[28] The zinc/MXene asymmetric MSC could operate in a voltage window of 1.1 V and exhibited a specific capacitance of 66.5 mF/cm^2.

In a simple alternating filtration method, a free-standing, highly flexible paper electrodes of MXene ($Ti_3C_2T_x$)/CNT were sandwiched through an aqueous suspension.[29] This paper electrode exhibited significantly high volumetric capacitance and excellent rate capabilities when compared to pure MXenes or randomly mixed MXene/CNT electrodes. Though no all-solid-state supercapacitor was demonstrated in this work, the paper electrode delivered a volumetric capacitance of 390 F cm^{-3} at a scan rate of 2 mV s^{-1}. Also, at 5 A g^{-1}, the electrode was able to deliver 350 F cm^{-3} for almost 10,000 cycles with no performance degradation.

2.3. 2D MXene Electrodes for Battery-Type Hybrid Supercapacitors

Though supercapacitors exhibit high power densities and long cycling life, low energy density is still a bottleneck for long term applications. On the other hand, batteries are superior for their high energy densities but poor in delivering high power and provides short cycle life. Hence a strategy of fabricating a battery-type hybrid supercapacitor by combining a supercapacitor electrode with a battery-type electrode can be a potential solution to the energy/power problems associated with their individual counter-parts. Hence both high energy and power densities can be attained in a single device. Another issue in fabricating a battery-type hybrid supercapacitor is the selection of electrolytes. The electrolyte should be feasible for both the supercapacitor electrode and the battery-type electrode; otherwise, it lacks synchronization in the charge storage and eventually leads to failure of the hybrid device. The aqueous electrolytes-based metal-ion hybrid supercapacitors utilizing a metal-based battery-type electrode in combination with a suitable supercapacitor electrode has achieved popularity in the recent past.[30] A recent review of the literature indicates that the MXenes are generally used as electrodes for supercapacitor applications but are achieving interest in batteries too.[31]

Aqueous electrolytes-based battery-type hybrid supercapacitors have several advantages like non-flammability, low-cost, environment friendliness, and safe handling. MXene-based battery-type hybrid supercapacitors are not explored to a great extent. An aqueous electrolyte-based battery-type zinc-ion hybrid supercapacitor was fabricated using MXene/rGO aerogel.[32] The zinc-ion hybrid supercapacitor was fabricated using porous $Ti_3C_2T_x$ MXene/rGO aerogel as the cathode, zinc

foil as the anode, and 2 M $ZnSO_4$ as the aqueous electrolyte. The MXene-rGO//Zn hybrid supercapacitor exhibited a high specific capacitance of 128.6 F/g and an energy density of 34.9 Wh/kg at a corresponding power density of 279.9 W/kg at a current density of 0.4 A/g. The ZHSC also showed an ultra-long cycle life of 75000 cycles with 95% capacitance retention.

3. Two-Dimensional Transition Metal Dichalcogenides (TMDs) in Supercapacitors

Transition metal dichalcogenides or TMDs, belong to a special group of two dimensional (2D) compounds with the formula MX_2 where, M is the transition metal atom (like Mo, W, etc.) and X is a chalcogen atom (like S, Se, or Te, etc.). TMD monolayer of MX_2 type is an atom thick and these different layers are held together by weak van der Walls interactions.[33,34] In a single MX_2 monolayer, the transition metal atom layer is sandwiched between two layers of chalcogen atoms via strong covalent bonds, which give rise to high strength for the monolayer.[34,35] These monolayers may be stacked upon each other, but they can be very easily exfoliated to a single layer of MX_2 nanosheet, which can benefit the capacitive behavior by increasing the storage space for electrolyte ions and also the contact area with electrolyte.[36]

When it comes to the application in supercapacitors, TMDs have been widely researched and have shown their potential as ideal energy storage materials. High specific surface area, conductivity and redox-active nature of the TMDs make them ideal for a fast charge-discharge supercapacitor.[37] Many TMDs show varied electronic structures ranging from superconductive materials ($TaSe_2$, $NbSe_2$), semi-metals (VS_2, TiS_2) to semiconductors (MoS_2, WS_2) and insulators (HfS_2).[38] This variation in electronic structure offers diversity to the work function of these materials, which in turn could help to design a high voltage device out of them. The predominant charge storage mechanism for these TMDs is still unclear. Some of them exhibit the electrical double layer capacitance (EDLC) mechanism, while others show pseudocapacitive behavior to store charges.[39]

3.1. 2D TMD Electrodes for Symmetric Supercapacitors

In the symmetric configuration of the supercapacitors, two identical electrodes are chosen as cathode and anode for assembling the device. When it comes to the application of TMDs for a symmetrical design in supercapacitors, many of them like MoS_2, WS_2, TiS_2, $MoSe_2$, etc. have been used to fabricate symmetrical devices.[40] However, compared to all other TMDs, MoS_2 has been the most widely explored because of its excellent, optoelectronic, nanoelectronic, energy harvesting and storage properties.[41] MoS_2 possesses nanosheets like structure which can provide a large surface area for a double layer charge storage mechanism.[42]

Recently, Neetika et al. have grown high-quality MoS_2 thin films, having nanoworms like structure, on a copper substrate using DC sputtering technique.[43] These films have been shown in Figure 6(a) and the SEM image of the nanoworms has been shown in Figure 6(b). DC sputtering technique is good for a large-scale uniform deposition with better adhesion properties, which does not require any polymer binder. Avoiding the use of a polymer binder (low conducting) not only helped to achieve higher gravimetric capacitance (by bringing a reduction in weight) but also led to a lower ESR value of 2.63 Ω in the EIS spectra for individual electrode tested in 1 M Na_2SO_4. Both EDLC and pseudocapacitance were responsible for the charge storage mechanism, as shown by the CV and GCD plots for single electrode electrochemical characterization in a 1 M Na_2SO_4 solution. However, no specific peaks in the CV curve signify the dominance of the EDLC mechanism over pseudocapacitance. For fabrication of a full-scale symmetric device, two MoS_2 working electrodes were assembled with a separator in between in aqueous 1 M Na_2SO_4 was used as an electrolyte. Similar to individual electrode study, various EC characterizations like CV, GCD and EIS were performed on the full-scale device. For CV studies, a range of 5–200 mV/s was chosen. This MoS_2 nanoworm symmetric device delivered specific capacitances of 152, 134, 107, 81, 65, and 48 F/g at scan rates of 5, 10, 20, 50, 100, and 200 mV/s, respectively. These CV plots are shown in Figure 6(c) and specific capacitance vs scan rate data is plotted in figure 6(d). Figure 6(e) shows the GCD plots of the symmetric device at different densities from 1–20 A/g. The triangular shape of the GCD curves with a voltage drop (IR drop) advocates the dominance of EDLC behavior. Specific capacitance was also calculated based on the GCD curves at different current densities which showed that the devices delivered high specific capacitances of 138, 112, 91, 68, and 38 F/g at current densities of 1, 2, 5, 10, and 20 A/g respectively. Energy density and power density of the symmetric device were calculated against each other at different values: 12.26 Wh/kg at 0.4 kW/kg, 9.95 Wh/kg at 0.8 kW/kg, 8.08 Wh/kg at 1.99 kW/kg, 6.04 Wh/kg at 3.99 kW/kg, and 3.37 Wh/kg at 7.98 kW/kg. The device showed a cycle life of about 5000 cycles at a scan rate of 200 mV/s and retained almost 86% of its capacitance. This little degradation in capacitance over cycling is owed to the absence of an ideal binder material during the fabrication process. Similar to the single electrode configuration, EIS was also performed on the full-scale symmetric device, which showed a low equivalent series resistance (R_s) of 3.35 Ω and charge transfer resistance of 7.09 Ω. This suggests an excellent ionic conductivity combined with fast ion adsorption due to the open pore structure of the MoS_2 nanoworm structure.

MoS_2 has also been used to fabricate MSC devices in the symmetric configuration by L.J. Cao et al. in 2013.[44] MoS_2 film based MSC were fabricated by spray painting of MoS_2 nanosheets on a Si/SiO_2 chip followed by a laser patterning process. Three different methodologies were adopted to synthesize different MoS_2 nano sheet-structures on the Si/SiO_2 substrate. First, MoS_2 paint was developed using an anionic sulfate assisted hydrothermal process and was denoted by h-MoS_2. In

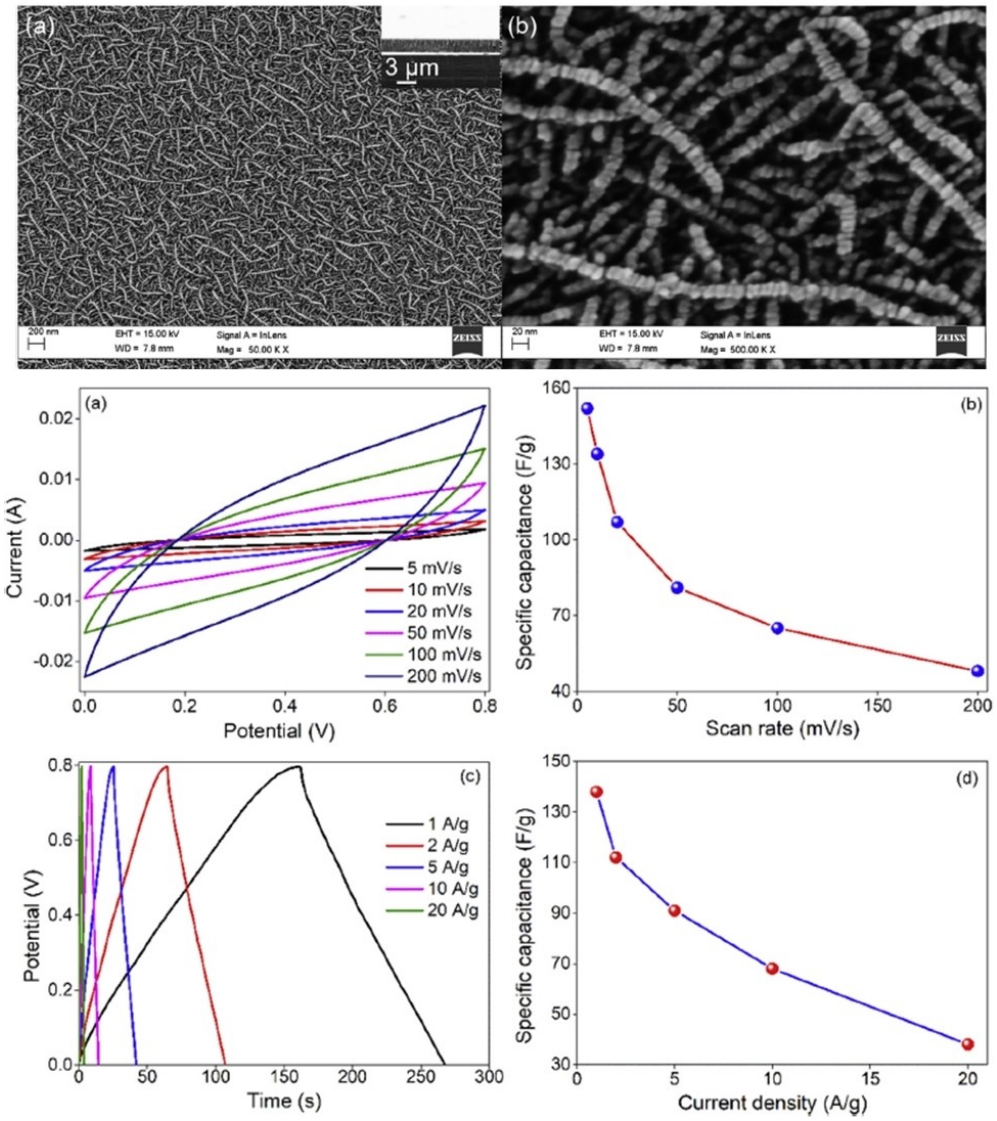

Figure 6. Low (a) and high (b) magnification FE-SEM image of MoS_2 nanoworms on copper substrates,[43] c) CV curves of MoS_2 symmetric device at different scan rates ranging from 5–200 mV/s in 1 M Na_2SO_4. d) Specific capacitances of MoS_2 symmetric device at different scan rates ranging from 5–200 mV/s in 1 M Na_2SO_4. e) GCD curves of MoS_2 symmetric device at different current densities from 1–20 Ag^{-1} in 1 M Na_2SO_4. f) Specific capacitances of MoS_2 symmetric device at different current densities ranging from 1–20 Ag^{-1} in 1 M Na_2SO_4. Reproduced with permission from Ref. [43]. Copyright (2018) Hydrogen Energy Publications LLC. Published by Elsevier Ltd.

the second methodology, the liquid exfoliation route was adopted and it was termed as e-MoS_2. The third methodology simply employed commercially available bulk MoS_2 powder to form the paint. Spray coating of h-MoS_2 resulted in a crumpled morphology with a layered structure of MoS_2 nanosheets while that of e-MoS_2 showed more flat and rigid films. MoS_2 bulk powder didn't show any specific structure. For these three different methodologies, three symmetric MSCs were carved out using laser patterning. From the electrochemical characterization (specifically CV) of the symmetric devices, it was found that specific areal capacitance of h-MoS_2 based device was the highest (~8 mF cm^{-2}) followed by that of e-MoS_2 (~3.1 mF cm^{-2}) and MoS_2 powder (~1.8 mF cm^{-2}). This performance data corroborated to the structure of MoS_2 coatings obtained via different methodologies. Even in terms of volumetric capacitance, h-MoS_2 delivered the highest performance of 178 F cm^{-3}. This superior performance of h-MoS_2 among the three reported structures owes to the fact that i) h-MoS_2 had a graphene-like open sheet structure that maximized the surface effect, unlike the bulk powdered MoS_2 and the restacked e-MoS_2 nano-sheets. This provided a large number of active sites for a fast and reversible surface redox reaction, giving pseudocapacitance. ii) Rough and layered morphology of h-MoS_2 resulted in larger pore size, which facilitated better ion movement from the electrolyte to the electrode.

MoS_2 is not the only TMD to be used in the fabrication of symmetric supercapacitors. Zhang et al.[45] in 2014 demonstrated Tin Selenide ($SnSe_2$) nanodisks-based all-solid-state flexible supercapacitors with symmetric configuration. They also studied different phases of $SnSe_2$ prepared via different

synthesis routes, which include: Pure $SnSe_2$ nanodisks (NDs), pure SnSe nanosheets (NSs), and a mixed-phase SnSe-$SnSe_2$ NDs. All these different phases were obtained by reacting different compositions of "$SnCl_2$ and trioctylphophine (TOP)" with "borane-tert-butylamine complex (BTBC) and 1,3-dimethyl-3,4,5,6-tetrahydro-2(1H)-pyrimidinone. Different phases of 2D-Tin Selenide were realized by the interplay of TOP and BTBC. Keeping the amount of TOP constant, the quantity of BTBC was varied to get three different phases. A very typical phase-dependent pseudocapacitive behavior was observed with the resulting 2D nanostructures. Further, the two distinct phases of $SnSe_2$ NDs and SnSe NSs were used to fabricate all-solid-state flexible symmetric supercapacitors (SSCs). Based on their phases, they were termed as $SnSe_2$ NDs-SSCs and SnSe NSs-SSCs. Different electrochemical characterizations like CV and GCD were performed for both devices. CV of $SnSe_2$ NDs-SSC was performed in the potential range -0.4 V to $+0.4$ V and no redox peak was observed, indicating no pseudocapacitive reaction. Therefore, energy storage in these electrodes takes palace by EDLC mechanism. Similarly, SnSe NSs-SSC was characterized through CV in the range -0.6 V to $+0.6$ V. In this case also, no redox peak was observed and the rectangular shape indicates EDLC mechanism for energy storage. The specific capacitances of both devices were accurately determined by GCD, which was performed at current densities ranging from 20 to 150 mAm^{-2}. For $SnSe_2$ NDs-SSC, almost 406 $\mu F\,cm^{-2}$ of areal capacitance was obtained at 20 mAm^{-2} current density and 250 $\mu F\,cm^{-2}$ of areal capacitance at 100 mAm^{-2}. On the other hand, SnSe NSs-SSC delivered a real capacitance of 442 $\mu F\,cm^{-2}$ at a current density of 100 mAm^{-2}, which is much higher than that of $SnSe_2$ NDs-SSC. However, in terms of rate capability, $SnSe_2$ NDs-SSC showed much superior performance than that of SnSe NSs-SSC.

3.2. 2D TMD Electrodes for Asymmetric Supercapacitors

As discussed previously, in the asymmetric configuration, two different electrode materials are chosen to overcome the limitation of the voltage window of the electrolyte.[46] The difference in the electrode work function value facilitates the enhancement of the voltage window, which in turn increases the capacitance as well as the energy density of the device. Many literature reports can be found which demonstrate the fabrication of asymmetric supercapacitors by using either two different TMDs or a TMD with another material (popularly carbon-based).[47,48]

Though different TMDs like MoS_2, VS_2, WS_2, and $MoSe_2$ have been frequently used to fabricate an asymmetric device, MoS_2 remains the most researched material for energy storage.[49] In 2016 Yang et al.[48] demonstrated an asymmetric supercapacitor with MnO_2 and MoS_2 flower-like growth on Graphene Nanosheets (GNS) as the positive and negative electrodes, respectively. The PVA-Na_2SO_4 gel was used as an electrolyte. Flower-like MoS_2/GNS and MnO_2/GNS electrodes were synthesized in a controlled manner using a hydrothermal approach. The MoS_2/GNS hybrid electrode typically exhibited crinkly and rippled structure with ultrathin MoS_2 nanosheets uniformly grown on graphene nanosheets in a flower-like arrangement. Figure 7(a) shows the SEM image of the MoS_2/GNS hybrid, while Figure 7 (b) shows the schematic diagram of the MoS_2 layered patches growing on GNS. MoS_2/GNS and MnO_2/GNS electrodes were also electrochemically characterized in a typical three-electrode setup in 1 M Na_2SO_4 aqueous electrolyte. For comparison of performance, the CV curves of both the electrodes were plotted together in Figure 7(c). Further, both MoS_2/GNS and MnO_2/GNS hybrid electrodes were dipped in the PVA-Na_2SO_4 gel electrolyte and assembled to form an asymmetric supercapacitor

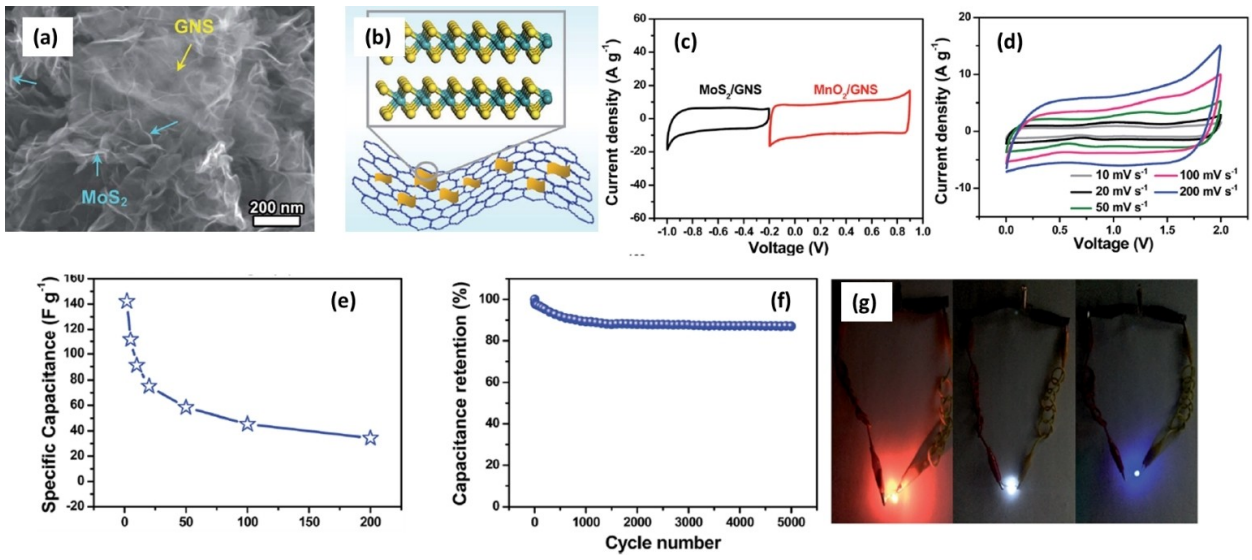

Figure 7. a) SEM image of MoS_2/GNS hybrid. b) Schematic diagram of MoS_2 growing on GNS. c) Comparative CV curves of MoS_2/GNS and MnO_2/GNS electrodes obtained in a three-electrode cell at 10 $mV\,s^{-1}$. d) CV curves of fabricated MnO_2/GNS//MoS_2/GNS ASC device measured at various scan rates in the voltage range of 0 to 2.0 V. e) Specific capacitance vs. scan rate (in $mV\,s^{-1}$) for fabricated MnO_2/GNS//MoS_2/GNS ASC device. f) Cycle performance of the ASC device measured at 100 $mV\,s^{-1}$ after 5000 cycles. g) Two assembled all-solid-state ASC devices connected in series to light up the commercial LEDs simultaneously. Reproduced with permission from Ref. [48]. Copyright (2016) The Royal Society of Chemistry.

(ASC) with cellulose paper as the separator between them. The CV curves of the fabricated ASC at different scan rates are given in Figure 7(d). The device showed a maximum specific capacitance of 142 $F g^{-1}$ at a scan rate of 2 $mV s^{-1}$. The assembled all-solid-state asymmetric device delivered an energy density of value 78.9 $W h Kg^{-1}$ at a power density value of 284.1 $W Kg^{-1}$.

MoS_2 has also been mixed with $MoSe_2$ to form heterojunctions exhibiting superior ion storage ability, enhancing the capacitive storage. Songzhan Li et al.[50] fabricated a 2D heterojunction of MoS_2 and $MoSe_2$ held together by van der Waals /covalent interaction. Since the topmost layer decides the work function and electronic states, the formation of this heterojunction gave high flexibility in modifying the electrochemical activity and ion storage performance. This heterojunction was based on 2D $MoSe_2$ nanoflakes and MoS_2 nanosheets and was synthesized using the epitaxial growth process. For fabrication of the asymmetric supercapacitor device, $MoSe_2/MoS_2$ synthesized heterostructure, as the positive electrode was assembled with metal-organic framework derived-nitrogen-doped carbon as a negative electrode. The $MoSe_2/MoS_2$//NC asymmetric supercapacitor exhibited a stable potential window of about 1.8 V. Though, other electrochemical performance parameters like specific capacitance, cycle life, energy and power density of the ASC have not been determined by the authors of this work, but for $MoSe_2/MoS_2$ heterostructure electrode, a high specific capacitance of 1229.6 $F g^{-1}$ at a current density of 1 $A g^{-1}$ was obtained. The electrode also showed an average cycle life of 2000 cycles with 92.8% capacitance retention.

In another work by Lin et al.,[51] a new class of ternary heterostructure using reduced graphene oxide, Molybdenum sulfide, and Tungsten sulfide was prepared by simple chemical synthesis. Through various characterization techniques like Raman and X-ray photoelectron spectroscopy (XPS), it was observed that a MoS_2/WS_2 heterostructure is uniformly deposited over a conductive rGO platform and offered a large surface area of about 109 $m^2 g^{-1}$. When tested as a supercapacitor electrode material, this MoS_2/WS_2/rGO heterostructure displayed a pseudocapacitive mechanism for charge storage in a 3 M KOH electrolyte solution. The MoS_2/WS_2/rGO ternary composite electrode exhibited a high specific capacitance of 365 $F g^{-1}$ at 1 $A g^{-1}$ current density, which is much higher when compared to the single TMD (like MoS_2, WS_2, etc.) composite. This enhancement in the electrochemical performance is attributed to TMDs' wide range of oxidation states, lower internal resistance due to the formation of a heterostructure of MoS_2/WS_2, and uniform arrangement of few-layer TMD nanosheets on the conductive rGO surface. In order to demonstrate its practical application, an asymmetric supercapacitor was assembled using MoS_2/WS_2/rGO ternary composite as the positive electrode and rGO as the negative electrode. From CV studies, it was observed that the device shows stable performance in the potential range of 0 to 1.6 V. Non-rectangular shape of CV indicated the pseudocapacitive mechanism of charge storage. From the CV, the device showed a maximum specific capacitance value of 85 $F g^{-1}$ at a slow scan rate of 5 $mV s^{-1}$. The maximum energy density achieved by the device was 15 $W h Kg^{-1}$ at a power density of 373 $W Kg^{-1}$. The cycling stability remained average, about 3000 cycles, with about 70% capacitance retention.

3.3. 2D TMD Electrodes for Battery-Type Hybrid Supercapacitors

Though TMDs have been very popularly used in supercapacitor applications in both symmetric and asymmetric type configurations when it comes to the battery type hybrids, barely any reports have been found for TMD based devices developed. In order to understand, what is a battery type hybrid, the total amount of charge storage in an ion intercalating type of energy storage device, can be divided into three categories. i) Non-Faradaic EDLC types of charge storage by electrostatic ion adsorption and desorption, ii) Faradaic, charge transfer type of storage by ions getting adsorbed on to the surface (also known as pseudocapacitance), iii) Faradaic, bulk solid-state ion diffusion (diffusion-controlled battery type process).[52] In any two-electrode configuration device, if one of the electrode stores charges via bulk solid-state ion diffusion, then it is a battery type electrode in a battery type hybrid device.

Though there are not many reports of battery type hybrid devices using TMDs, in 2016, Liu et al.[53] fabricated a battery hybrid electrode of net-like $MoSe_2$-acetylene black (AB) on nickel foam (substrate) using a simple facile hydrothermal strategy by tailoring the interior of the substrate. Figure 8 (A) shows pristine nickel foam of almost 4 cm wide. Figure 8 (B), (C), and (D) show hydrothermally deposited $MoSe_2$-AB/Ni electrode and its bendability by almost 45^0. The unique nanowall structure of $MoSe_2$-AB grown on the nickel foam can be seen in the SEM image of Figure 8(E), which also shows that the TMD layer has uniformly grown on even in the interiors of the nickel foam, forming a bulk type structure that can facilitate solid-state ion diffusion leading to a battery type mechanism in charge storage. This can also be observed through the high-density TEM image in Figure 8(F). Both SEM and TEM images show the well interconnected $MoSe_2$ network grown on Nickel foam with a uniform and average pore diameter of 50 to 150 nm, which in turn acts as a growing site for $MoSe_2$ and AB nanosheets. Electrochemical studies of $MoSe_2$-AB/Ni and $MoSe_2$-AB electrodes (for comparison) were performed in a 3-electrode setup in a 6 M KOH electrolyte. Figure 8(G) shows CV curves of the $MoSe_2$–AB, $MoSe_2$–AB/Ni at 50 $mV s^{-1}$ scan rate with clear and identifiable redox peaks at −0.1 V and −0.4 V, while Figure 8(H) showed CV curves for $MoSe_2$–AB/Ni electrode at different scan rates. In order to investigate the mechanism of charge storage using the relation $i_p = a\ v^b$ where a and b are adjustable parameters and i_p is the peak current (in mA) while v is the scan rate (in mVs^{-1}), $log\ i_p$ vs $log\ v$ curve has been plotted in Figure 8(I). From this curve, b value (slope) has been calculated. If the b value is closer to 0.5, it shows a diffusion-controlled (battery type) charge storage mechanism, while at a value closer to 1, reflects surface type (capacitive) charge storage mechanism. The b values obtained in their study are

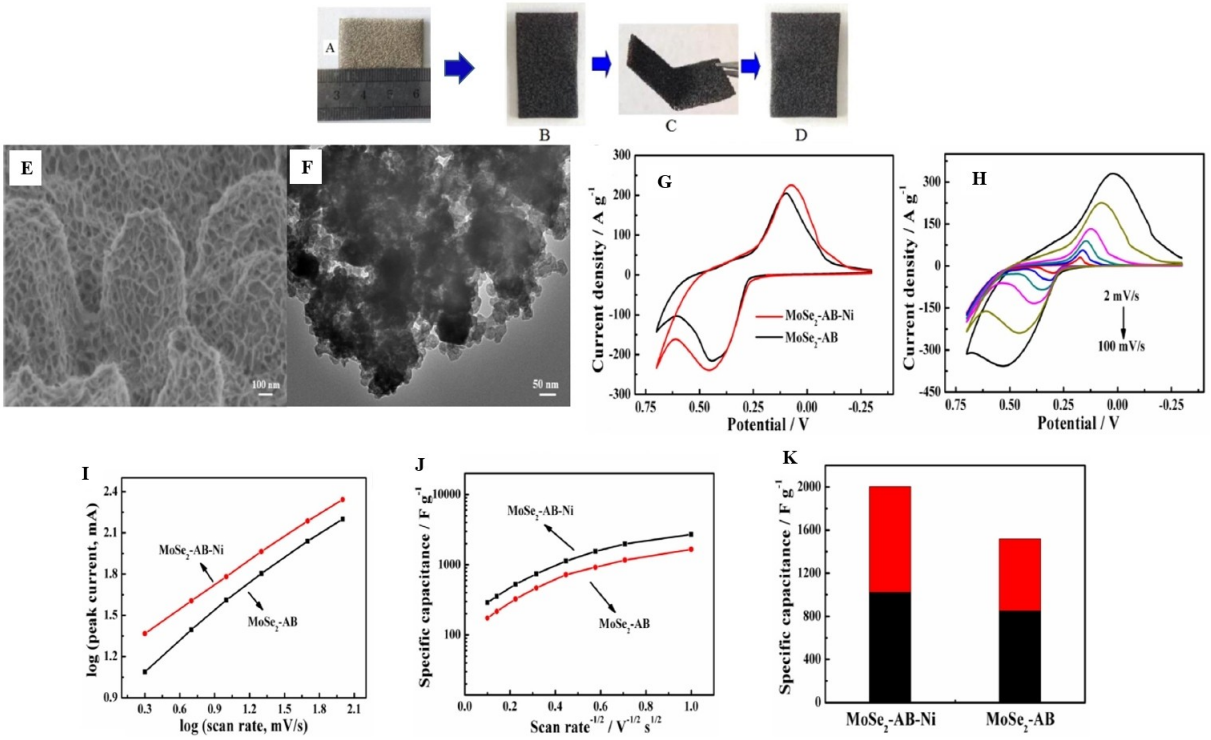

Figure 8. A–D): Pristine Nickel Foam, $MoSe_2$–AB grown nickel foam, Bended $MoSe_2$–AB/Ni electrode, and re-straightened $MoSe_2$–AB/Ni electrode respectively. E) and F) SEM and TEM image of $MoSe_2$–AB/Ni electrode at a scale bar of 100 nm and 50 nm, respectively. G) CV curves of the $MoSe_2$–AB, $MoSe_2$–AB/Ni at 50 mV s^{-1} in 6.0 M KOH. H) CV curves of the $MoSe_2$–AB/Ni composite at different scan rates (2, 5, 10, 20, 50 and 100 mV s^{-1}). I) Log *i* vs Log *v* curves to find the slope for calculation of *b*. J) Specific capacitance vs. scan rate for $MoSe_2$–AB and $MoSe_2$–AB/Ni electrodes. K) Contribution of surface (capacitive) "Black"- and diffusion-controlled (battery hybrid) "Red" charge transfer kinetics in $MoSe_2$–AB and $MoSe_2$–AB/Ni electrodes. Reproduced with permission from Ref. [53]. Copyright (2016) Elsevier B.V.

0.65 and 0.59 for $MoSe_2$–AB and $MoSe_2$–AB/Ni, respectively. This means that the $MoSe_2$–AB/Ni electrode stores a good amount of bulk diffusion-controlled charge. The individual contributions of capacitive charge storage and battery type (diffusion-controlled) charge storage for $MoSe_2$–AB/Ni and $MoSe_2$–AB is given in Figure 8(K). From the GCD studies of $MoSe_2$–AB/Ni electrode, it was found that $MoSe_2$-AB composite exhibited a very high specific capacitance of 2020 F g^{-1} at a current density of 1 A g^{-1} and also showed a very good cycling ability of 1500 cycles retaining 107.5 % of its capacitance.

4. Two-Dimensional Phosphorene in Supercapacitors

Phosphorene is an emerging 2D material that consists of a single atomic layer of black phosphorus.[54] Black phosphorus is like graphite, black in color, flaky nature, and layered structure and layers bonded via weak Van der Walls force. It is analogous to graphene and exhibits excellent unique properties such as good electronic conductivity, thermal stability, tensile strength, ionic transport, etc.[55] It has comparable characteristics when compared with other 2D materials such as graphene and TMDs. Due to its peculiar properties, they found applications in field-effect transistors,[56] rechargeable batteries,[57] optoelectronic devices,[58] supercapacitors,„[59] etc. This section briefly discusses the recent developments in the phosphorene/few-layered black phosphorus-based symmetric and asymmetric hybrid supercapacitors. Hybrid electrodes prepared using black/red phosphorous via. the sonochemical process is found to be a potential candidate for application in supercapacitors in the recent past.[60] Pristine phosphorene electrodes exhibit low specific capacitance and also face a major challenge of self-restacking, composite electrodes have been prepared.[61]

4.1. 2D Phosphorene-Based Symmetric Hybrid Supercapacitors

Liquid-exfoliated black-phosphorus nanoflakes deposited on platinum-coated PET substrate were used as electrodes to fabricate an all-solid-state symmetric supercapacitor with polyvinyl alcohol/H_3PO_4 gel polymer electrolyte.[62] The same research group has also reported the fabrication of flexible all-solid-state symmetric supercapacitor using black-phosphorus nanoflakes/carbon nanotubes composite paper electrodes and polyvinyl alcohol/H_3PO_4 gel polymer electrolyte.[63] The as-fabricated symmetric device exhibited a specific capacitance of 41.1 F/cm^3 at a scan rate of 0.005 V/s and retained a capacitance of 35.7 F/cm^3 even after 11 months. The symmetric device was able to deliver a power density of 821.62 W/cm^3

with a corresponding energy density of 5.71 mWh/cm^3. A comparison of the performance of phosphorene nanoflakes/carbon nanotube-based symmetric supercapacitor with other 2D materials-based supercapacitors and other energy storage devices is depicted in Figure 9. This asymmetric device possessed high mechanical flexibility and long cycle life of 10000 cycles with 91.5 % capacitance retention.

MSC s with interdigitated electrodes have advantages such as small size, flexibility, high voltage, scalability, etc.[64] Interdigital MSC were fabricated with interdigital phosphorene/graphene hybrid electrodes with high energy density.[59] This interdigital MSC delivered a maximum areal capacitance of ~9.8 mF/cm^2 and a volumetric capacitance of 37.0 F/cm^3 at a scan rate of 5 mV/s. A high energy density of 11.6 mWh/cm^3 is also obtained for the MSC. The interdigital MSC could work with a high cell voltage of 3 V in an electrolyte consisting of ionic liquid of 1-butyl-3-methylimidazolium hexafluorophosphate. The electrochemical performance of the phosphorene/graphene hybrid electrodes-based MSC was superior to those fabricated with pristine graphene and phosphorene MSCs. This study revealed that the preparation of all-2D hybrid electrodes consisting of graphene and phosphorene is a suitable candidate for high-performance supercapacitors. Another advantage of such all-2D electrodes is that they prevent the possible self-restacking of the phosphorene nanosheets. This, in turn, helps in retaining the porous structure within the electrode nanostructure, which in turn facilitates the fast ion-transport and eventually boosts the charge storage capability. A similar strategy was adopted to prepare hybrid electrodes consisting of a few-layer exfoliated black phosphorous (H_xPO_y) and rGO flakes.[65] The H_xPO_y/rGO hybrid supercapacitor exhibited a specific capacitance of 104.4 F/g at a current density of 0.25 A g^{-1} in 1 M H_3PO_4 aqueous electrolyte. The relaxation time for the H_xPO_y/rGO hybrid supercapacitor was 0.31 s, whereas it was 1.8 s for the pristine rGO supercapacitor, which indicates that the former possessed superior rate capability when compared to the latter.

Redox polymer, polypyrrole, was used in the fabrication of an all-solid-state supercapacitor with black phosphorus nanosheets and PVA/H_3PO_4 solid-state polymer electrolyte.[66] The concentration of black phosphorous in preparing the free-standing electrodes consisting of polypyrrole/black phosphorous laminated films was found critical in determining the conductivity of the said electrodes; more concentration led to a decrease in the conductivity. The polypyrrole/black phosphorous symmetric supercapacitor exhibited good electrochemical charge storage, evident from Figure 10a. The charge/discharge curves show good reversibility (Figure 10b) and good capacitance retention, even at a severe bending angle of 180° (Figure 10c). The all-solid-state device underwent 3000 bending cycles at an angle from 0 to 135° and no obvious degradation was observed (Figure 10d). The symmetric device exhibited good cycling life of 12000 cycles without any significant degradation in its capacitance (Figure 10e) and is fully flexible (Figure 10f) and is a potential candidate in the next-generation flexible and wearable supercapacitors.

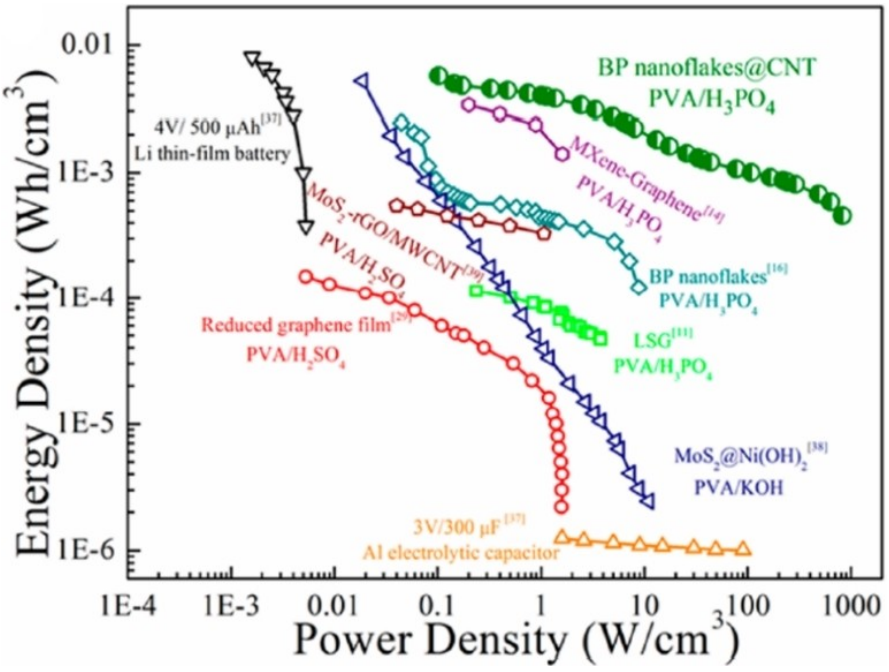

Figure 9. Ragone plot of all-solid-state phosphorene nanoflakes/carbon nanotube symmetric supercapacitor device, compared with other 2D electrode materials-based supercapacitors and commercial energy storage systems. Reproduced with permission from Ref. [63]. Copyright (2017) American Chemical Society.

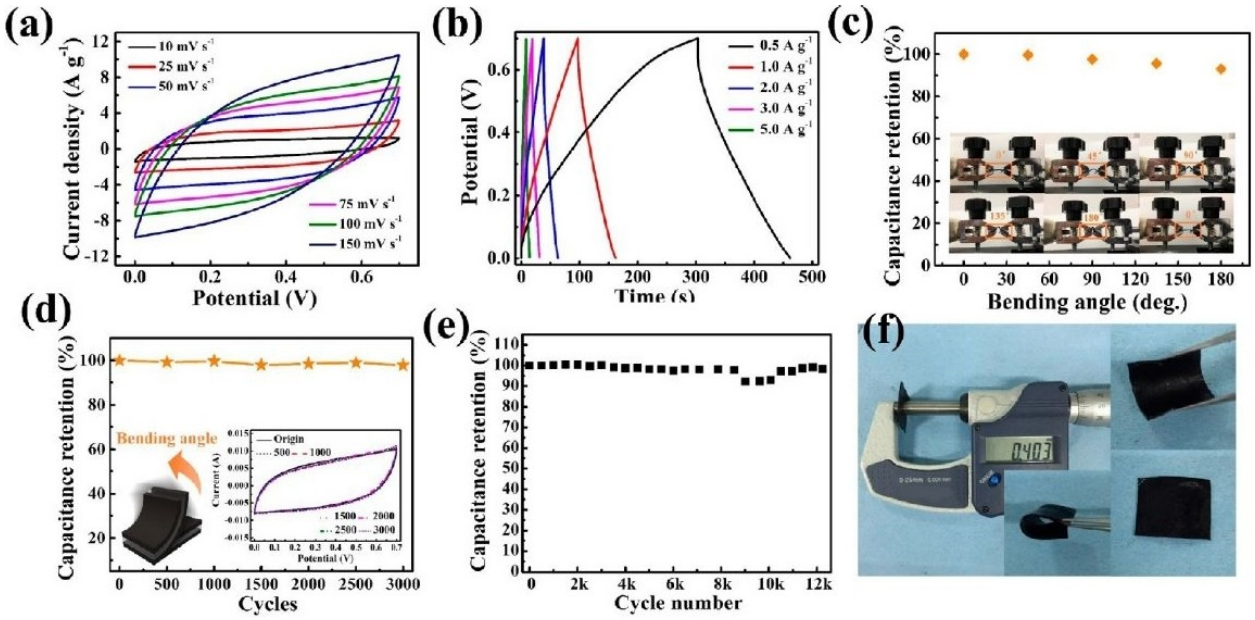

Figure 10. The electrochemical performance of the all-solid-state polypyrrole/black phosphorous symmetric supercapacitor: a) CV curves at different scan rates, b) GCD curves at different current densities, c) plot of capacitance retention at different bending angles, d) plot of capacitance retention at different bending cycles, e) plot of capacitance retention at different cycle numbers, and f) digital photographs showing the flexibility of the all-solid-state polypyrrole/black phosphorous symmetric supercapacitor. Reproduced with permission from Ref. [66]. Copyright (2018) American Chemical Society.

4.2. 2D Phosphorene-Based Asymmetric Hybrid Supercapacitors

A review of the literature shows that there are limited research articles published in the field of asymmetric hybrid supercapacitors manufactured with phosphorene electrodes. The charge balance between the two electrodes (positive and negative) is very important in obtaining good electrochemical performance to the asymmetric supercapacitor device. Either the electrode mass or the electrode area should be adjusted to obtain the required charge balance. Electrochemical cathode exfoliation is a viable technique to synthesize large surface area bearing few-layered phosphorene nanosheets from black phosphorous.[67] Electrochemical cathode exfoliated phosphorene is found to exhibit excellent charge storage capabilities with a high electrode capacitance of 3181.5 F/g.[68] It was further used as a cathode for fabricating an asymmetric supercapacitor using polyaniline based anode and 1 M H_2SO_4/0.5 M KI aqueous electrolyte. A maximum specific energy density of 203.7 Wh/kg was obtained for the asymmetric hybrid supercapacitor and possessed a stable cycling life of 1000 cycles with 100% capacitance retention. The enhanced charge exchange performance of this supercapacitor was explained due to the possession of movable lone pair electrons of the phosphorous atoms in the electric field.

5. 2D Materials Summary, Prospects and Challenges

Due to their layered structure, 2D materials like TMDs, MXenes, and phosphorenes have already shown their high potentials for future energy storage applications. These 2D materials have revolutionized the research in the field of flexible and wearable energy storage systems. This includes both batteries and supercapacitors. However, each of these materials has certain advantages and challenges that need to be scrutinized.

MXenes are a large family of layered 2D carbides, carbonitrides and nitrides which are prepared by selective etching and exfoliation of layered ternary precursors. This synthesis process attaches hydroxyl, oxygen, and fluorine terminations to its surfaces, making them hydrophilic. This hydrophilicity and a negative surface charge (negative zeta-potential beyond −30 mV) give these layers an ability to form water-stable colloidal solutions, without the addition of any surfactant. This makes the processing of MXenes very easy and facilitating them to be used for device printing, coatings, and uniform film depositions using a simple spray or spin-coating techniques. Besides, these MXenes films and polymer-bonded MXenes exhibit high mechanical strength and flexural rigidity, which is appropriate for their usage in flexible supercapacitors. Some MXenes like $Ti_3C_2T_x$ have shown metallic conductivities even with their surface-functionalization and adsorbed water molecules in between the layers. Also, the spacing between the interlayers of MXenes can be intercalated with cations and polar organic molecules. The combination of high electronic conductivity, controlled interlayer spacing for intercalation, and the presence of redox-active transition metal atom make

MXenes an ideal choice for supercapacitor electrodes. However, there exist many drawbacks and challenges that need to be addressed. MXenes are synthesized by etching MAX phase, which removes main group elements like Al and Si. Hence it becomes challenging to identify the termination group through techniques like XRD, EDAX, or NMR spectroscopy. Often these termination groups are uncontrollable, and MXenes with uniform surface termination groups, i.e., with the same kind of surface moieties (like hydroxyl, fluorine, oxygen, or hydrogen), have been very difficult to be synthesized. MXenes with no functional group are yet to be produced.

TMDs are a class of material that is very thin and are similar to graphene. When it comes to flexible energy storage applications, they have numerous advantages. The thin-layered structure of TMDs offers very short electron transport length and short ion diffusion lengths. This could enable them to exhibit fast charge/discharge cycles, which is ideal for their application in supercapacitors. The surface of 2D TMDs shows both "faradaic" and "non-faradaic" charge storage mechanisms. This results in higher and efficient usage of the surface area, leading to better cycling performance and higher energy density. Moreover, these surfaces possess catalytically active edges that can be appropriately developed into energy storage sites by introducing conversion reactions. Not only the surface but also the bulk TMDs can show a fast ion exchange, that too with metal ions larger than Li^+, because of their wider interlayer spacing. Besides these, TMDs exhibit good surface tunability and rich coordination sites, which helps in full utilization of the areal and volumetric capacities. The thin layered structure of 2D TMDs also gives them the ability to yield to high bending angles, making them a perfect candidate for flexible supercapacitors. However, there are certain drawbacks and challenges that need to be addressed if TMDs have to make their way to the market. Many TMDs (1H/2H phases in particular) are very difficult to synthesize as monolayers. Their fabrication generally ends up in reduced yield, making large scale production almost impossible.

On the other hand, 2D 1T-TMDs are thermally unstable. There have been no technological advancements to develop 2D 1T-TMDs, which are stable and have good electrical conductivity. Similar electrical conductivity issues arise with 1H/2H phases. Though they might be better in terms of stability when compared to 1T phase, their poor electrical conductivities impede their use in high-performance energy storage devices.

2D phosphorenes are a new class of materials that are currently being investigated for their potential in flexible supercapacitors. Their assembly with CNT or graphene leads to increased volumetric capacity and provides elastic buffer spacing. Meanwhile, 1D CNT and 2D graphene facilitate in faster electron transport from the redox reaction occurring in phosphorine, to the current collector. This 2D phosphorene is very effective in adsorbing and trapping polysulfides, which can enhance the electrochemical performance of Li–S battery hybrid electrodes, for a flexible battery hybrid supercapacitors. Besides these advantages, research on 2D phosphorene as energy storage material is still in its early stages. Many pushbacks are needed to be resolved. There has been no known technology for large scale production of phosphorene. Moreover, there is hardly any literature available to control the phosphorene thickness or its electrochemical properties. Therefore uniformity of layers remains a significant challenge while synthesizing phosphorene. Pristine 2D phosphorene also exhibits low stability in open air and moisture. However, this can be countered using a passivation layer deposition of BN, Al_2O_3, MoS_2, etc. This passivation layer can not only block air exposure but also can alleviate volumetric changes during cycling. The volumetric energy density of pristine 2D phosphorine based devices still remains low, owing to the inferior packing densities of 2D materials. However, synthesizing nanocomposites of phosphorene with other carbonaceous materials can help to achieve higher packing densities. Also, doping with heterogeneous atoms can help to increase the low specific capacitance by introducing redox pseudocapacitance.

6. Conclusions and Future Perspectives

In this review, we have discussed the recent developments made in 2D materials-based electrodes in supercapacitor applications. The electrochemical properties of 2D electrode materials such as MXenes, transition metal dichalcogenides, phosphorene, and their composites for supercapacitors are discussed in detail. The successful implementation of 2D electrode materials in various supercapacitor configurations such as symmetric, asymmetric, and battery-type hybrids are emphasized to get an insight into the relevance of each category for the desired output. 2D materials are attractive materials for supercapacitors as they possess unique features such as large surface area, good electrochemical activity, and highly-reactive surface edges. Fast-electrolyte diffusion through the tiny pores created between the 2D materials leads to faster electrode kinetics, which enables high specific capacitance and energy densities.

MXenes were discovered very recently, in 2011. Therefore, there are many open questions that need to be answered before they can be utilized to their full extent. Any layered structure of transition metal carbide/nitride, having $M_{n+1}X_n$ layers that are separated by A-group metals or A-carbide/nitrides, can be selectively etched and exfoliated, to be qualified and put into the category of MXenes. Because of this, though, many computational studies have been performed, their ternary carbide precursors, like Sc_2C, Hf_2C, and W_2C, are yet to be produced. These computational studies have already started predicting the electrochemical characteristics of upcoming new MXenes. Thus experimental verification is needed for these predictions. Understanding of ion dynamics between the MXene sheets is required for the fabrication of high power supercapacitors. 2D TMDs with their metallic 1T phases have demonstrated high electronic conductivity, which is more than 10^7 times of the semiconducting 2H phase. They also possess high hydrophilicity, which enhances the adsorption of aqueous electrolyte ions. However, new techniques are required to increase both the phase yield (which is around 70% using the chemical exfoliation method) and the stability. Suitable chem-

ical doping can be used to stabilize the 1T phase. On the other hand, more stable but less conducting 1H/2H phases can be used to fabricate hybrids with vertically aligned graphene or other conducting materials to enhance its electronic conductivity and facilitate the pseudocapacitive reactions. Another hybrid with graphene as a platform to support 2D TMDs nanocrystals, loaded in between the channels of graphene, could also be considered to avoid the inefficacies of electron transfer between 2D TMDs layers. This structure can also increase porosity for efficient ion diffusion. When it comes to 2D phosphorene, it's a very new and emerging material which has very intriguing properties. Since it is rather new material, it requires more research to investigate its electrochemical properties. There is no known literature regarding a dedicated study for suitable and safe electrolytes, binder materials, etc. which are appropriate for phosphorene based electrodes.

The current post graphene era is witnessing a wide variety and hybrids of 2D materials, which are not only electrochemically superior to their parent structure but also cheap and becoming scalable. All-2D supercapacitors using electrodes prepared by combining two different 2D materials, for example, graphene and phosphorene, have several advantages such as obtaining high-specific capacitance, restricting self-restacking issues of the 2D nanosheets, enhancing ion intercalation/diffusion, etc. The preparation of composite electrodes helps in utilizing the synergistic effects of the individual components to attain high-performance in supercapacitors. The 2D materials-based flexible supercapacitors are promising for next-generation flexible and wearable electronic devices.

Acknowledgements

J.T. acknowledges National Science Foundation for the CAREER supplement award (1351757) for the partial completion of this work.

Conflict of Interest

The authors declare no conflict of interest.

Keywords: 2D materials · Symmetric · Asymmetric · Battery-Hybrid · Supercapacitor

[1] J. Mohtasham, *Energy Procedia* **2015**, *74*, 1289.
[2] A. Demirbaş, *Energy Sources* **2006**, *28*, 779.
[3] a) J. Cherusseri, K. K. Kar, *J. Mater. Chem. A* **2016**, *4*, 9910; b) J. Cherusseri, K. K. Kar, *J. Mater. Chem. A* **2015**, *3*, 21586; c) C. Li, M. M. Islam, J. Moore, J. Sleppy, C. Morrison, K. Konstantinov, S. X. Dou, C. Renduchintala, J. Thomas, *Nat. Commun.* **2016**, *7*, 13319.
[4] a) H. Hu, Z. Pei, C. Ye, *Energy Storage Mater.* **2015**, *1*, 82; b) D. S. Gardner, C. W. Holzwarth III, Y. Liu, S. B. Clendenning, W. Jin, B.-K. Moon, C. Pint, Z. Chen, E. C. Hannah, C. Chen, *Nano Energy* **2016**, *25*, 68; c) C. Shen, S. Xu, Y. Xie, M. Sanghadasa, X. Wang, L. Lin, *J. Microelectromech. Syst.* **2017**, *26*, 949.
[5] a) A. Chu, P. Braatz, *J. Power Sources* **2002**, *112*, 236; b) A. Burke, H. Zhao, "Applications of supercapacitors in electric and hybrid vehicles", presented at *ITS*, **2015**.
[6] a) J. Cherusseri, R. Sharma, K. K. Kar, *Carbon* **2016**, *105*, 113; b) B. Duong, Z. N. Yu, P. Gangopadhyay, S. Seraphin, N. Peyghambarian, J. Thomas, *Adv. Mater. Interfaces* **2014**, *1*.
[7] a) T. Qin, *Batteries & Supercaps* **2019**, *2*, 948; Supercaps **2019**, 2, 948; b) B. Krüner, C. Odenwald, A. Quade, G. Kickelbick, V. Presser, *Batteries & Supercaps* **2018**, *1*, 135; c) P. Zhang, L. Wang, F. Wang, D. Tan, G. Wang, S. Yang, M. Yu, J. Zhang, X. Feng, *Batteries & Supercaps* **2019**, *2*, 918; Supercaps **2019**, 2, 918.
[8] Z. Xiao, S. Wang, X. Yan, C. Liu, X. Zhao, X. Yang, *Batteries & Supercaps* **2019**, *2*, 766; Supercaps **2019**, 2, 766.
[9] a) J. Cherusseri, K. K. Kar, *RSC Adv.* **2015**, *5*, 34335; b) Z. Yu, M. McInnis, J. Calderon, S. Seal, L. Zhai, J. Thomas, *Nano Energy* **2015**, *11*, 611.
[10] a) K. Sambath Kumar, J. Cherusseri, J. Thomas, *ACS Omega* **2019**, *4*, 4472; b) J. Cherusseri, R. Sharma, K. K. Kar, in *Handbook of polymer nanocomposites. Processing, performance and application*, Springer, **2015**, 479.
[11] J. Cherusseri, K. Sambath Kumar, D. Pandey, E. Barrios, J. Thomas, *Small* **2019**, *1902606*.
[12] S. J. Varma, K. S. Kumar, S. Seal, S. Rajaraman, J. Thomas, *Adv. Sci.* **2018**, *5*.
[13] a) M. Naguib, O. Mashtalir, J. Carle, V. Presser, J. Lu, L. Hultman, Y. Gogotsi, M. W. Barsoum, *ACS Nano* **2012**, *6*, 1322; b) M. Naguib, V. N. Mochalin, M. W. Barsoum, Y. Gogotsi, *Adv. Mater.* **2014**, *26*, 992; c) G. R. Bhimanapati, Z. Lin, V. Meunier, Y. Jung, J. Cha, S. Das, D. Xiao, Y. Son, M. S. Strano, V. R. Cooper, *ACS Nano* **2015**, *9*, 11509.
[14] a) M. Naguib, J. Come, B. Dyatkin, V. Presser, P.-L. Taberna, P. Simon, M. W. Barsoum, Y. Gogotsi, *Electrochem. Commun.* **2012**, *16*, 61; b) S. J. Kim, M. Naguib, M. Zhao, C. Zhang, H.-T. Jung, M. W. Barsoum, Y. Gogotsi, *Electrochim. Acta* **2015**, *163*, 246; c) Y. Xie, M. Naguib, V. N. Mochalin, M. W. Barsoum, Y. Gogotsi, X. Yu, K.-W. Nam, X.-Q. Yang, A. I. Kolesnikov, P. R. Kent, *J. Am. Chem. Soc.* **2014**, *136*, 6385; d) M. R. Lukatskaya, O. Mashtalir, C. E. Ren, Y. Dall'Agnese, P. Rozier, P. L. Taberna, M. Naguib, P. Simon, M. W. Barsoum, Y. Gogotsi, *Science* **2013**, *341*, 1502; e) Z. Ling, C. E. Ren, M.-Q. Zhao, J. Yang, J. M. Giammarco, J. Qiu, M. W. Barsoum, Y. Gogotsi, *Proc. Natl. Acad. Sci. USA* **2014**, *111*, 16676.
[15] R. B. Rakhi, B. Ahmed, M. N. Hedhili, D. H. Anjum, H. N. Alshareef, *Chem. Mater.* **2015**, *27*, 5314.
[16] Y. Tian, C. Yang, W. Que, X. Liu, X. Yin, L. B. Kong, *J. Power Sources* **2017**, *359*, 332.
[17] R. B. Rakhi, B. Ahmed, D. Anjum, H. N. Alshareef, *ACS Appl. Mater. Interfaces* **2016**, *8*, 18806.
[18] a) C. Yu, P. Ma, X. Zhou, A. Wang, T. Qian, S. Wu, Q. Chen, *ACS Appl. Mater. Interfaces* **2014**, *6*, 17937; b) Y. Huang, J. Tao, W. Meng, M. Zhu, Y. Huang, Y. Fu, Y. Gao, C. Zhi, *Nano Energy* **2015**, *11*, 518; c) A. Sumboja, U. M. Tefashe, G. Wittstock, P. S. Lee, *Adv. Mater. Interfaces* **2015**, *2*, 1400154.
[19] M. Zhu, Y. Huang, Q. Deng, J. Zhou, Z. Pei, Q. Xue, Y. Huang, Z. Wang, H. Li, Q. Huang, *Adv. Energy Mater.* **2016**, *6*, 1600969.
[20] S. Jiao, A. Zhou, M. Wu, H. Hu, *Adv. Sci.* **2019**, *6*, 1900529.
[21] Y.-Y. Peng, B. Akuzum, N. Kurra, M.-Q. Zhao, M. Alhabeb, B. Anasori, E. C. Kumbur, H. N. Alshareef, M.-D. Ger, Y. Gogotsi, *Energy Environ. Sci.* **2016**, *9*, 2847.
[22] H. Hu, T. Hua, *J. Mater. Chem. A* **2017**, *5*, 19639.
[23] M. Boota, Y. Gogotsi, *Adv. Energy Mater.* **2019**, *9*, 1802917.
[24] Q. Jiang, N. Kurra, M. Alhabeb, Y. Gogotsi, H. N. Alshareef, *Adv. Energy Mater.* **2018**, *8*, 1703043.
[25] R. Liu, A. Zhang, J. Tang, J. Tian, W. Huang, J. Cai, C. Barrow, W. Yang, J. Liu, *Chem. Eur. J* **2019**, *25*, 5547.
[26] Z. Wang, S. Qin, S. Seyedin, J. Zhang, J. Wang, A. Levitt, N. Li, C. Haines, R. Ovalle-Robles, W. Lei, *Small* **2018**, *14*, 1802225.
[27] Y. Wang, X. Wang, X. Li, Y. Bai, H. Xiao, Y. Liu, R. Liu, G. Yuan, *Adv. Funct. Mater.* **2019**, *29*, 1900326.
[28] N. Wang, J. Liu, Y. Zhao, M. Hu, R. Qin, G. Shan, *ChemNanoMat* **2019**, *5*, 658.
[29] M. Q. Zhao, C. E. Ren, Z. Ling, M. R. Lukatskaya, C. Zhang, K. L. Van Aken, M. W. Barsoum, Y. Gogotsi, *Adv. Mater.* **2015**, *27*, 339.
[30] a) J.-G. Wang, Z. Zhang, X. Zhang, X. Yin, X. Li, X. Liu, F. Kang, B. Wei, *Nano Energy* **2017**, *39*, 647; b) B. Li, F. Dai, Q. Xiao, L. Yang, J. Shen, C. Zhang, M. Cai, *Energy Environ. Sci.* **2016**, *9*, 102; c) S. Amaresh, K. Karthikeyan, I.-C. Jang, Y. Lee, *J. Mater. Chem. A* **2014**, *2*, 11099.
[31] a) X. Tang, X. Guo, W. Wu, G. Wang, *Adv. Energy Mater.* **2018**, *8*, 1801897; b) V. Shukla, N. K. Jena, S. R. Naqvi, W. Luo, R. Ahuja, *Nano Energy* **2019**, *58*, 877.

[32] Q. Wang, S. Wang, X. Guo, L. Ruan, N. Wei, Y. Ma, J. Li, M. Wang, W. Li, W. Zeng, *Adv. Electron. Mater.* **2019**, *1900537*.
[33] N. A. Kumar, M. A. Dar, R. Gul, J.-B. Baek, *Mater. Today* **2015**, *18*, 286.
[34] a) A. H. Loo, A. Bonanni, Z. Sofer, M. Pumera, *Electrochem. Commun.* **2015**, *50*, 39; b) C. C. Mayorga-Martinez, A. Ambrosi, A. Y. S. Eng, Z. Sofer, M. Pumera, *Electrochem. Commun.* **2015**, *56*, 24.
[35] a) M. Yousaf, Y. Wang, Y. Chen, Z. Wang, W. Aftab, A. Mahmood, W. Wang, S. Guo, R. P. Han, *ACS Appl. Mater. Interfaces* **2018**, *10*, 14622; b) S. K. Balasingam, J. S. Lee, Y. Jun, *Dalton Trans.* **2015**, *44*, 15491.
[36] a) Y. Chao, R. Jalili, Y. Ge, C. Wang, T. Zheng, K. Shu, G. G. Wallace, *Adv. Funct. Mater.* **2017**, *27*, 1700234; b) X. Zhang, L. Hou, A. Ciesielski, P. Samorì, *Adv. Energy Mater.* **2016**, *6*, 1600671.
[37] a) H. Wang, H. Feng, J. Li, *Small* **2014**, *10*, 2165; b) M.-R. Gao, Y.-F. Xu, J. Jiang, S.-H. Yu, *Chem. Soc. Rev.* **2013**, *42*, 2986; c) C. Rao, K. Gopalakrishnan, U. Maitra, *ACS Appl. Mater. Interfaces* **2015**, *7*, 7809.
[38] a) Q. H. Wang, K. Kalantar-Zadeh, A. Kis, J. N. Coleman, M. S. Strano, *Nat. Nanotechnol.* **2012**, *7*, 699; b) M. Chhowalla, H. S. Shin, G. Eda, L.-J. Li, K. P. Loh, H. Zhang, *Nat. Chem.* **2013**, *5*, 263.
[39] a) B. E. Conway, V. Birss, J. Wojtowicz, *J. Power Sources* **1997**, *66*, 1; b) B. E. Conway, *J. Electrochem. Soc.* **1991**, *138*, 1539.
[40] M. A. Bissett, S. D. Worrall, I. A. Kinloch, R. A. Dryfe, *Electrochim. Acta* **2016**, *201*, 30.
[41] K.-J. Huang, L. Wang, Y.-J. Liu, Y.-M. Liu, H.-B. Wang, T. Gan, L.-L. Wang, *Int. J. Hydrogen Energy* **2013**, *38*, 14027.
[42] a) M. Kim, Y. K. Kim, J. Kim, S. Cho, G. Lee, J. Jang, *RSC Adv.* **2016**, *6*, 27460; b) C. M. Smyth, R. Addou, S. McDonnell, C. L. Hinkle, R. M. Wallace, *J. Phys. Chem. C* **2016**, *120*, 14719.
[43] A. Sanger, V. K. Malik, R. Chandra, *Int. J. Hydrogen Energy* **2018**, *43*, 11141.
[44] L. Cao, S. Yang, W. Gao, Z. Liu, Y. Gong, L. Ma, G. Shi, S. Lei, Y. Zhang, S. Zhang, *Small* **2013**, *9*, 2905.
[45] C. Zhang, H. Yin, M. Han, Z. Dai, H. Pang, Y. Zheng, Y.-Q. Lan, J. Bao, J. Zhu, *ACS Nano* **2014**, *8*, 3761.
[46] J. Chang, M. Jin, F. Yao, T. H. Kim, V. T. Le, H. Yue, F. Gunes, B. Li, A. Ghosh, S. Xie, *Adv. Funct. Mater.* **2013**, *23*, 5074.
[47] a) T. M. Masikhwa, F. Barzegar, J. K. Dangbegnon, A. Bello, M. J. Madito, D. Momodu, N. Manyala, *RSC Adv.* **2016**, *6*, 38990; b) M. Rantho, M. Madito, F. Ochai-Ejeh, N. Manyala, *Electrochim. Acta* **2018**, *260*, 11.
[48] X. Yang, H. Niu, H. Jiang, Q. Wang, F. Qu, *J. Mater. Chem. A* **2016**, *4*, 11264.
[49] J. Theerthagiri, R. Senthil, B. Senthilkumar, A. R. Polu, J. Madhavan, M. Ashokkumar, *J. Solid State Chem.* **2017**, *252*, 43.
[50] S. Li, W. Zang, X. Liu, S. J. Pennycook, Z. Kou, C. Yang, C. Guan, J. Wang, *Chem. Eng. J.* **2019**, *359*, 1419.
[51] T. W. Lin, T. Sadhasivam, A. Y. Wang, T. Y. Chen, J. Y. Lin, L. D. Shao, *ChemElectroChem* **2018**, *5*, 1024.
[52] J. Wang, J. Polleux, J. Lim, B. Dunn, *J. Phys. Chem. C* **2007**, *111*, 14925.
[53] X. Liu, J.-Z. Zhang, K.-J. Huang, P. Hao, *Chem. Eng. J.* **2016**, *302*, 437.
[54] A. Khandelwal, K. Mani, M. H. Karigerasi, I. Lahiri, *Mater. Sci. Eng. B* **2017**, *221*, 17.
[55] M. C. Watts, L. Picco, F. S. Russell-Pavier, P. L. Cullen, T. S. Miller, S. P. Bartuś, O. D. Payton, N. T. Skipper, V. Tileli, C. A. Howard, *Nature* **2019**, *568*, 216.
[56] a) H. Liu, Y. Du, Y. Deng, D. Y. Peide, *Chem. Soc. Rev.* **2015**, *44*, 2732. b) L. Li, Y. Yu, G. J. Ye, Q. Ge, X. Ou, H. Wu, D. Feng, X. H. Chen, Y. Zhang, *Nat. Nanotechnol.* **2014**, *9*, 372.
[57] W. Li, Y. Yang, G. Zhang, Y.-W. Zhang, *Nano Lett.* **2015**, *15*, 1691.
[58] a) J. Dai, X. C. Zeng, *J. Phys. Chem. Lett.* **2014**, *5*, 1289; b) Z. Guo, W. Ding, X. Liu, Z. Sun, L. Wei, *Appl. Mater. Today* **2019**, *14*, 51.
[59] H. Xiao, Z.-S. Wu, L. Chen, F. Zhou, S. Zheng, W. Ren, H.-M. Cheng, X. Bao, *ACS Nano* **2017**, *11*, 7284.
[60] X. Chen, G. Xu, X. Ren, Z. Li, X. Qi, K. Huang, H. Zhang, Z. Huang, J. Zhong, *J. Mater. Chem. A* **2017**, *5*, 6581.
[61] A. Sajedi-Moghaddam, C. C. Mayorga-Martinez, Z. K. Sofer, D. Bouša, E. Saievar-Iranizad, M. Pumera, *J. Phys. Chem. C* **2017**, *121*, 20532.
[62] C. Hao, B. Yang, F. Wen, J. Xiang, L. Li, W. Wang, Z. Zeng, B. Xu, Z. Zhao, Z. Liu, *Adv. Mater.* **2016**, *28*, 3194.
[63] B. Yang, C. Hao, F. Wen, B. Wang, C. Mu, J. Xiang, L. Li, B. Xu, Z. Zhao, Z. Liu, *ACS Appl. Mater. Interfaces* **2017**, *9*, 44478.
[64] D. Qi, Y. Liu, Z. Liu, L. Zhang, X. Chen, *Adv. Mater.* **2017**, *29*, 1602802.
[65] J. Cao, P. He, J. R. Brent, H. Yilmaz, D. J. Lewis, I. A. Kinloch, B. Derby, *ACS Appl. Mater. Interfaces* **2018**, *10*, 10330.
[66] S. Luo, J. Zhao, J. Zou, Z. He, C. Xu, F. Liu, Y. Huang, L. Dong, L. Wang, H. Zhang, *ACS Appl. Mater. Interfaces* **2018**, *10*, 3538.
[67] H. Xiao, M. Zhao, J. Zhang, X. Ma, J. Zhang, T. Hu, T. Tang, J. Jia, H. Wu, *Electrochem. Commun.* **2018**, *89*, 10.
[68] L. Zu, X. Gao, H. Lian, C. Li, Q. Liang, Y. Liang, X. Cui, Y. Liu, X. Wang, X. Cui, *J. Alloys Compd.* **2019**, *770*, 26.

Manuscript received: December 31, 2019
Revised manuscript received: April 27, 2020
Accepted manuscript online: April 28, 2020
Version of record online: June 4, 2020